Measurement and Modeling of the Millimeter-Wave Backscatter Response of Soil Surfaces

Adib Nashashibi, *Member, IEEE,* Fawwaz T. Ulaby, *Fellow, IEEE,* and Kamal Sarabandi, *Senior Member, IEEE*

***Abstract*—The millimeter-wave (MMW) backscatter response of bare-soil was examined by conducting experimental measurements at 35 and 94 GHz using a truck-mounted polarimetric scatterometer and by developing appropriate models to relate the backscattering coefficient to the soil's surface and volume properties. The experimental measurements were conducted for three soil surfaces with different roughnesses under both dry and wet conditions. The experimental measurements indicate that in general the backscattering coefficient is comprised of a surface scattering component σ^s and a volume scattering component σ^v. For wet soil conditions, the backscatter is dominated by surface scattering, while for dry conditions both surface and volume scattering are significant, particularly at 94 GHz. Because theoretical surface scattering models were found incapable of predicting the measured backscatter, a semiempirical surface scattering model was developed that relates the surface scattering component of the total backscatter to the roughness parameter ks, where $k = 2\pi/\lambda$ and s is the rms height, and the dielectric constant of the soil surface. Volume scattering was modeled using radiative transfer theory with the packed soil particles acting as the host material and the air voids as the scattering particles. The combined contribution of surface and volume scattering was found to provide good agreement between the model calculations and the experimental observations.**

I. Introduction

An extensive experimental investigation was conducted over the past three years to examine the polarimetric backscatter behavior of bare soil surfaces in the 1–10 GHz frequency range [1]. Using a set of truck mounted coherent polarimetric scatterometers with center frequencies at 1.25, 4.75, and 9.5 GHz, measurements were made of the Mueller matrix as a function of incidence angle for soil surfaces covering wide ranges of surface roughness and moisture content. Using the relations outlined in [1] and [2], the measured Mueller matrices were then used to compute the copolarized backscattering coefficients σ^o_{vv} and σ^o_{hh}, the cross-polarized backscattering coefficient σ^o_{hv}, and the probability density functions of the copolarized and cross-polarized phase differences. Comparison of the measured data with calculations based on the physical optics model, the geometric optics model, and the small perturbation method revealed that all three models are incapable of correctly predicting the backscatter response of random rough surfaces, even when applied within their presumed ranges of validity. This realization led Oh *et al.* [1] to develop a semiempirical model that relates σ^o_{ij}, for $i, j = h$ or v, to the incidence angle θ and the surface parameters ks and ϵ_r, where $k = 2\pi/\lambda$, s is the rms height and ϵ_r is the complex relative dielectric constant. The semiempirical model, which was developed on the basis of measurements made during one season of experimental observations, was found to provide excellent agreement not only with observations made during two succeeding years for different sets of soil surfaces and conditions, but it also provided a reasonable match to experimental observations reported by Yamasaki *et al.* [3] for wet soil surfaces at 60 GHz.

This paper extends the preceding work by examining the backscatter response of soil surfaces at millimeter wavelengths (MMW), specifically 35 and 94 GHz. One of the major lessons learned from the present study is that at centimeter wavelengths, it is reasonable to assume that the backscatter from a half-space soil medium is due to scatter by the soil surface alone, but at millimeter wavelengths the backscatter may consist of both surface and volume scattering contributions. Furthermore, for dry soils, the volume-scattering component may be comparable to or greater than the surface-scattering component, but for wet soil, the volume scattering component becomes negligibly small in comparison with the surface-scattering component. This behavior is consistent with calculations based on radiative transfer theory.

The next section contains detailed descriptions of the 35- and 94-GHz radar systems, the measurement procedure, and the measured properties of the soil surfaces. Section III provides an overview of the observed angular variation of σ^o for various surface roughnesses and introduces a scattering model composed of two terms, corresponding to surface and volume scattering contributions. The surface-scattering term is a semiempirical expression that provides a better fit to the data than the expression previously derived by Oh *et al.* [1] for surface scattering at centimeter wavelengths. Section IV examines the evidence for volume scattering and introduces a method for evaluating the volume-scattering term based on a numerical solution of the radiative transfer equation for a medium in which the soil particles are considered to be the host material and the air voids are the scatterers.

II. Experimental Setup

The first part of this section provides a brief description of the polarimetric scatterometers used in support of the present study. It is then followed with discussions of the techniques employed in preparing the surfaces and the methods

Manuscript received November 18, 1994; revised May 11, 1995.

The authors are with the Radiation Laboratory, Department of Electrical Engineering and Computer Science, University of Michigan, Ann Arbor, MI 48109 USA.

Publisher Item Identifier S 0196-2892(96)01013-3.

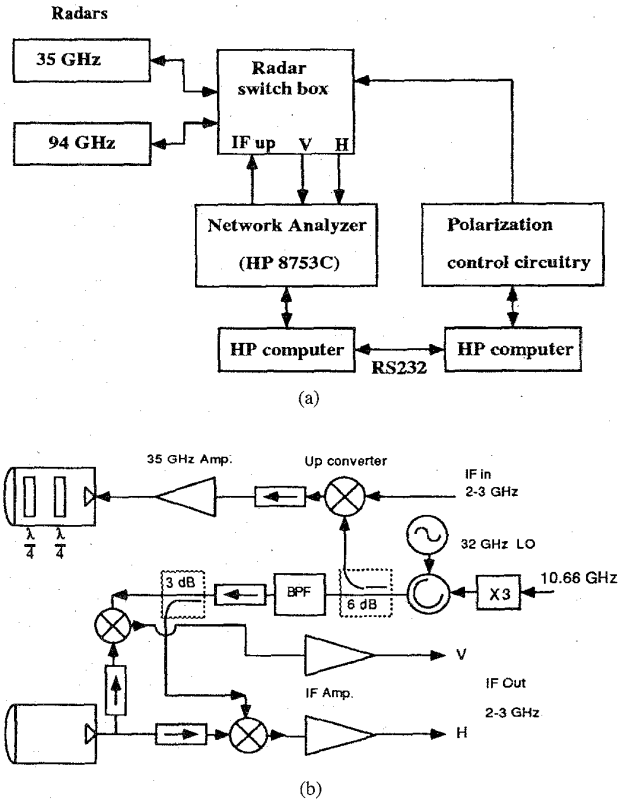

Fig. 1. Overview diagram of the MMW polarimetric radar system. (a) System block diagram. (b) RF front end circuitry of the 35-GHz radar.

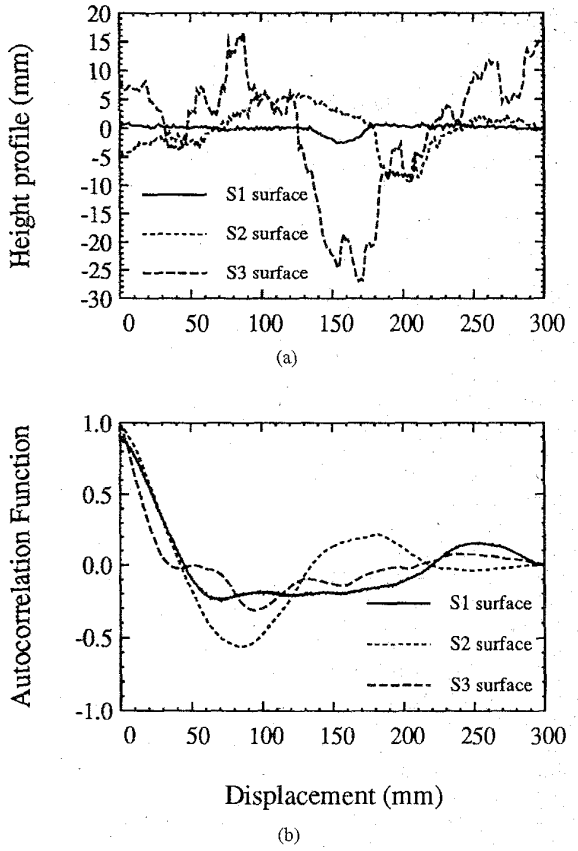

Fig. 2. (a) Samples of the surface height profiles, measured using a laser profiler. (b) Autocorrelation functions of the three surfaces.

used in characterizing the physical properties of the observed surfaces.

A. Polarimetric Scatterometer System

Two fully polarimetric truck-mounted scatterometer systems operating at 35 GHz and 94 GHz were used to conduct the experiments reported in this paper. A block diagram of the overall system, as well as the RF front-end circuitry of the 35 GHz radar, are shown in Fig. 1. The scatterometers are capable of measuring directly the Mueller matrix of a distributed target using the coherent-on-receive (COR) technique, [4]. With the COR technique, 4 to 6 different polarizations (V, H, 45L, LHC, 135L, and RHC) are transmitted sequentially. Each radar is capable of simultaneous detection of the vertical and horizontal components of the backscattered signal, preserving the phase-difference between the two components. The Stokes vector of the scattered field is recorded for each transmitted polarization and then the Mueller matrix of the target is determined from the ensemble averages of the measured Stokes vectors, following the procedure outlined by Ulaby *et al.* [4], [5].

The calibration of the scatterometers was performed in two steps. First, the receiver was calibrated using an odd-bounce reflector (a metallic sphere) and a polarizing grid placed in front of the receiving antenna. The receiver distortion matrix was determined by making the measurements with the polarizer positioned at each of three different angles. Second, the actually transmitted polarizations were determined using the calibrated receiver and the odd-bounce reflector. More details on the calibration technique are given in [6].

TABLE I
SURFACE ROUGHNESS STATISTICAL PARAMETERS FOR THE THREE SOIL SURFACES

surface	$s(mm)$	$l(mm)$	Freq(GHz)	ks	kl
S1	0.66	27	35	0.48	19.8
			94	1.3	53
S2	2.62	30	35	1.92	22
			94	5.16	59
S3	7.77	20	35	5.69	14.7
			94	15.3	39.4

s = rms height
l = correlation length
$k = 2\pi / \lambda$

B. Surface Preparation and Characterization

The wavelengths corresponding to 35 and 94 GHz are 8.6 and 3.2 mm, respectively. To insure that the backscattering measurements cover a wide range of surface roughness relative to λ, special care was taken in preparing the three soil surfaces. Initially, all the surfaces were cleared from grass and vegetation debris. Then, in order to have a "smooth" surface with rms height less than 1 mm, a heavy roller was moved across surface S1. This technique resulted in a compacted soil medium with an rms height $s = 0.66$ mm. Surface S2

TABLE II
SUMMARY OF SOIL PROPERTIES

					m_v		ϵ_r	
Surface	ρ_b	ν_a	d_p mm	d_v mm	0-1 cm	2-3 cm	35 GHz	94 GHz
S1-dry	1.69	0.36	0.3	0.165	0.02	0.08	(3.1, 0.05)	(3.1, 0.05)
S1-wet	1.69	0.36	0.3	0.165	0.23	0.19	(7.3,4.5)	(5.0,2.4)
S2-dry	1.37	0.45	0.3	0.165	0.04	0.07	(2.5, 0.05)	(2.5, 0.05)
S2-wet	1.37	0.45	0.3	0.165	0.12	0.12	(4.6,2.0)	(3.5,1.1)
S3-dry	1.32	0.50	0.3	0.242	0.04	0.07	(2.5, 0.05)	(2.5, 0.05)
S3-wet	1.32	0.50	0.3	0.242	0.19	0.18	(5.9,3.5)	(4.1,1.9)

ρ_b = soil bulk density (g/cm^3).
ν_a = air-voids volume fraction.
d_p = mean soil particle diameter.
d_v = mean air-void diameter.
m_v = volumetric moisture content.
ϵ_r = effective dielectric constant.

was a slightly rough surface with $s = 2.62$ mm, and for surface S3 the top layer was turned over by a hand shovel resulting in an undulating surface with $s = 7.77$ mm. Surface height characterization was performed by a laser profiler, as will be discussed later. Samples of surface profiles of the three surfaces and their autocorrelation functions are shown in Fig. 2. A summary of the roughness parameters for the three surfaces is given in Table I. Two sets of measurements were conducted, one for dry soil conditions and the other for wet soil conditions (see Table II).

For each soil surface, the radar backscatter data was collected at incidence angles of 20°, 45°, and 70° , under wet and dry soil conditions. For all observations, the distance from the radars to the surfaces was kept at about 10 m. At normal incidence, the antenna spot sizes for the 35 and 94-GHz radars were 0.6 and 0.3 m, respectively. Furthermore, to achieve good statistical representation of the measured backscatter, sixty independent spatial samples were collected for each surface. Additional independent samples were obtained by frequency averaging over the 1-GHz bandwidth. Overall, between 120 samples at $\theta = 20°$ and 240 samples at $\theta = 70°$ were collected for each target.

Although both the backscattering coefficients, σ^o_{vv}, σ^o_{hh}, and σ^o_{hv}, and the statistics of the phase-differences, ϕ_{hh-vv} and ϕ_{hv-vv}, can easily be derived from the Mueller matrix [7], only the backscattering coefficients are discussed in this paper. The measured phase-difference statistics are the subject of a separate report.

The height profile of each soil surface was measured by a laser profiler mounted on an x-y table. The profiler, which is driven by stepper motors, measured 30-cm long linear segments with 0.3 mm horizontal resolution and 0.3 mm vertical resolution. At least five height profiles of different areas were recorded for each surface. The rms height s and correlation length l are listed in Table I for each of the three surfaces.

The soil particle size distribution is shown in Fig. 3(a), indicating that the bulk of the soil material consists of fine sand (diameter $\geq$0.02 mm). To investigate the void size distribution of the soil medium, thin soil slices were collected and then photographed by a microscope camera. Two histograms of the void-size distribution were generated, one for bulk soil density $\rho_b = 1.69$ g/cm^3 (for soil surface S1) and another for $\rho_b = 1.32$ g/cm^3 (for soil surface S3), by treating the voids as spherical in shape. The mean void diameter was calculated to be 0.165 mm for the high-density soil, compared to 0.242 mm for the low-density soil. The void size distribution of the soil with $\rho_b = 1.69$ g/cm^3 is shown in Fig. 3(b).

In conjunction with the radar measurements, the soil bulk density ρ_b and the volumetric moisture content m_v were measured by collecting 1-cm thick soil samples for each of the top 3-cm soil layers. The average values of ρ_b and m_v are listed in Table II, for all three surfaces.

In order to compare the radar observations to theoretical models, we need to obtain good estimates of the soil's dielectric constant or relate the dielectric constant to the soil's physical properties. Unfortunately, no theoretical or empirical model is available in the literature that can correctly predict the effective dielectric constant of soils at MMW frequencies. In this paper, the effective dielectric constant of the soils observed in this study were estimated by applying the semiempirical formula found in [8] and [9]. The results are given in Table II. For the measured dry surfaces with low moisture content, it is difficult to determine accurately the amount of free water. In addition, it was observed that the first few millimeters of the soil medium were very dry, and the soil wetness increased gradually with depth. The values given in Table II for the dielectric constants of the dry soil surfaces are for the very top surface layer. The thickness of that dry surface layer plays an important role in determining the relative contribution of volume scattering to the total backscatter, as discussed later in Section IV-C.

III. SURFACE SCATTERING

This section examines the experimental behavior of the backscattering coefficient σ^o as a function of (1) the radar parameters: frequency, receive-transmit polarization configuration, and the incidence angle θ, and (2) the soil surface parameters: the rms surface height s, the surface correlation length l, and moisture content m_v. Where appropriate, semiempirical

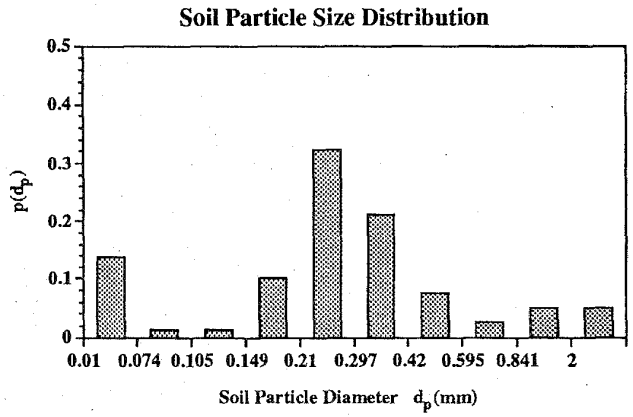

(a)

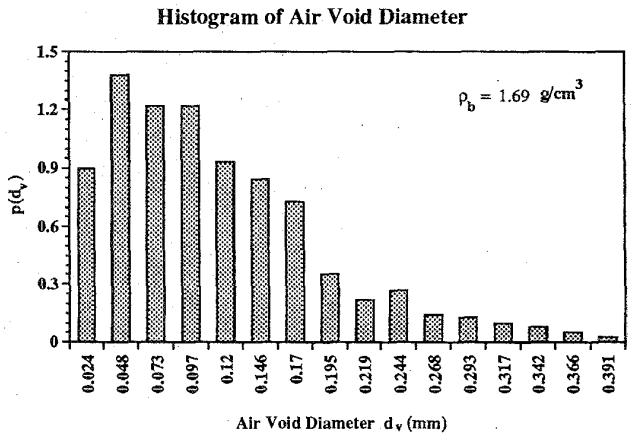

(b)

Fig. 3. Histogram of (a) soil particle size distribution $p(d_p)$ and (b) void-size distribution $p(d_v)$ for the soil with $\rho_b = 1.69$ g/cm^3.

expressions are introduced to characterize the observed radar response. This is done in lieu of using theoretical models because comparison of the measured data with values calculated in accordance with the commonly available scattering models (small perturbation, physical optics, and geometric optics) reveals poor agreement between the theoretical predictions and the experimental observations, as shown in Fig. 4(a) for the smoothest surface at 35 GHz, whose roughness parameters fall in the validity range of the physical optics model, and in Fig. 4(b) for the other two surfaces at 94 GHz, for which the geometric optics model is supposed to be applicable.

In general, two scattering mechanisms contribute to the backscattering coefficient σ^o (Fig. 5), a surface scattering contribution σ^s which is a function of the surface height statistics and ϵ_r of the lower half space, and a volume scattering contribution σ^v that is due to inclusions underneath the rough interface:

$$\sigma^o_{ij} = \sigma^s_{ij} + \sigma^v_{ij} \qquad i,j = h \text{ or } v. \tag{1}$$

The volume scattering contribution is in turn governed by the height statistics of the rough interface and the size and shape distributions of the inclusions in the soil medium (air voids in this case) and the dielectric constant of the host material (soil particles). Calculations based on radiative transfer theory reveal that σ^v is much smaller than the observed scattering coefficient σ^o, and hence much smaller than σ^s, except for dry soil at 94 GHz. This can be explained by noting that at 35 GHz the air voids are very small in size (see Fig. 3(b)) relative to λ, and at 94 GHz the attenuation in wet soil reduces the penetration depth to a very thin surface layer, thereby reducing the volume scattering contribution to a negligible level. First, we will limit the analysis to the wet soil cases in order to examine the surface scattering component alone and then we will use radiative transfer theory to model the volume-scattering component (Section IV). Hence, for the cases presented in this section, $\sigma^o = \sigma^s$.

As was stated earlier, the radar observations were made at 35 and 94 GHz for each of three surfaces with widely different roughnesses. Fig. 6 displays the angular variation of σ^o, for each of the three principal polarization configurations, for the surface with the smallest value of ks (surface S1 with $s = 0.66$ mm, observed at 35 GHz) and the surface with the largest value of ks (surface S3 with $s = 7.77$ mm, observed at 94 GHz). We note that the curves for the copolarized scattering coefficients, σ^o_{vv} and σ^o_{hh}, diverge as a function of θ for the smooth surface represented by Fig. 6(a), but they remain approximately equal for the very rough surface represented by Fig. 6(b). This behavior is consistant with previous observations made at centimeter wavelengths [1]. We also note that the difference in level between the σ^o_{vv} and σ^o_{hv} curves is at least 18 dB for the smooth surface (actually 21 dB at 20°, decreasing to 18 dB at 70°), whereas the difference never exceeds 13 dB for the very rough surface. These observations clearly indicate that surface roughness exercises a significant influence on both the copolarized ratio $p = \sigma^s_{hh}/\sigma^s_{vv}$ and the cross-polarized ratio $q = \sigma^s_{hv}/\sigma^s_{vv}$. It should be noted that the continuous curves shown in Fig. 6 are based on the semiempirical expressions introduced later in this section.

The three surfaces examined in this study were prepared to replicate a wide range of naturally occuring surface roughness conditions. Surface S1 represents a packed-down dirt road surface, surface S3 represents a freshly plowed soil surface, and S2 represents what surface S3 would look like after cultivation by a farm implement to break down the large soil clods or after natural smoothing action by rain and wind. An examination of Table I shows that among the three surfaces, the surface correlation length l varies over a narrower range of 1.5 : 1 (between a minimum of 2 cm for S3 and a maximum of 3 cm for S2). The corresponding range on the kl scale (where $k = 2\pi/\lambda$), is approximately 4 : 1. In contrast, the rms height s varies over a range of 12 : 1, and ks covers the range 32 : 1. A third surface roughness parameter of interest is the ratio $m = s/l$ which is equal to or proportional to the rms slope of the surface, with the proportionality constant being determined by the form of the surface autocorrelation function. For the three surfaces, m varies from 0.025 for S1 to 0.39 for S2. A detailed analysis was conducted to determine the sensitivities of the backscattering coefficients σ^o_{vv}, σ^o_{hh}, and σ^o_{hv} to s, l, ks, kl, and m. Plots of the backscattering coefficients *versus* the

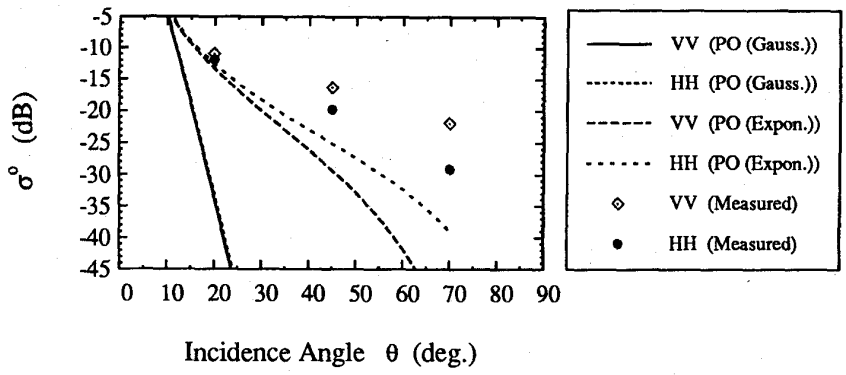

(a)

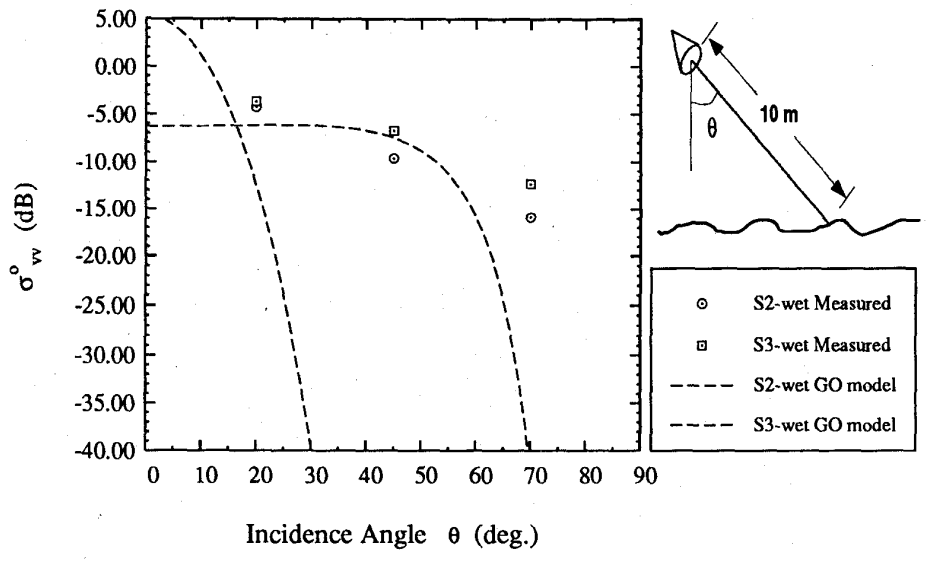

(b)

Fig. 4. Comparison between (a) measured data for surface S1 and predictions based on the physical optics (PO) model at 35 GHz for both Gaussian and exponential surface height autocorrelation functions, and (b) measured data for surfaces S2 and S3 and predictions based on the geometric optics (GO) model at 94 GHz.

five surface roughness descriptors revealed the following: a) strong but different dependences on s at 35 GHz and 94 GHz; b) the individual frequency plots coincide with each other when the data is plotted against ks; c) random variations with l and kl; and d) the variation with m is driven by the dependence on s. Considering that l exhibits a relatively narrow range among the three surfaces, it is not surprising that s was found to be the primary parameter governing the dependence of the radar backscatter on surface roughness.

A. Copolarization Ratio

The dependences of the co- and cross-polarized ratios p and q on ks are illustrated in Fig. 7. At $\theta = 20°$, p exhibits no discernible dependence on ks, as expected, because θ is close to normal incidence. At the higher angles of 45° and 70°, p increases with increasing ks until ks reaches a value of 4, beyond which p assumes the constant ratio of 1.0. The continuous curves shown in Fig. 7(a) are based on the following expression:

$$p = \frac{\sigma^s_{hh}}{\sigma^s_{vv}} = \left[1 - \left(\frac{2\theta}{\pi}\right)^{1/(3\Gamma_o)} \exp[-0.4ks]\right]^2 \quad (2)$$

where θ is the incidence angle in radians and Γ_o is the reflectivity for normal incidence,

$$\Gamma_o = \left|\frac{1-\sqrt{\epsilon_r}}{1+\sqrt{\epsilon_r}}\right|^2. \quad (3)$$

The form of (2), which was adapted from the experience gained previously from the centimeter-wave study [1], includes a dependence on the dielectric constant ϵ_r. The plots shown in Fig. 7(a) correspond to $\epsilon_r = 5.07 + j2.56$, which is in the middle of the range of the dielectric constants corresponding to the wet-soil surfaces observed by the radar (see Table II). Thus, part of the data scatter in Fig. 7(a) is attributed to the nonuniformity of dielectric constants among the data points.

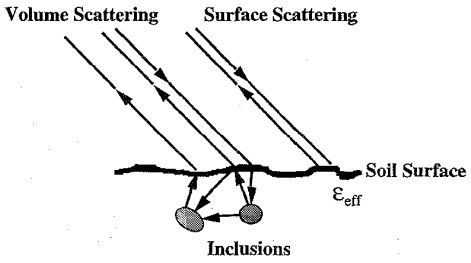

Fig. 5. Surface and volume-scattering mechanisms contributing to the total backscatter.

B. Cross-Polarization Ratio

The cross-polarization ratio q, which exhibits an inverse negative exponential dependence on ks for all angles of incidence (Fig. 7(b)), is modeled by the expression

$$q = \frac{\sigma^s_{hv}}{\sigma^s_{vv}} = 0.23\sqrt{\Gamma_o}\,[1 - \exp(-0.5\sin\theta\, ks)]. \quad (4)$$

To eliminate the dependence on the dielectric constant ϵ_r, the ratio q shown in Fig. 7(b) has been normalized by dividing it by $\Gamma_o^{1/2}$ for both the data points and the expression given by (4).

C. σ^s_{vv} Response

So far we have characterized the ratios of σ^s_{hh} and σ^s_{hv} with respect to σ^s_{vv} through (2) and (4). Now, we turn our attention to the response of σ^s_{vv} to θ, ks and ϵ_r. The proposed functional form is

$$\sigma^s_{vv} = g\,\frac{\cos^x\theta}{\sqrt{p}}\,[\Gamma_v(\theta) + \Gamma_h(\theta)] \quad (5)$$

where p is given by (2), $\Gamma_v(\theta)$ and $\Gamma_h(\theta)$ are the Fresnel reflectivities at incidence angle θ for v and h polarizations, respectively, and the function g is given by

$$g = 2.2(1 - \exp[-0.2ks]). \quad (6)$$

The exponent of the $\cos\theta$ term in (5) accounts for the change in the angular dependency of σ^s_{vv} as a function of ks, and is given by

$$x = 3.5 + \frac{1}{\pi}\,tan^{-1}[10\,(1.65 - ks)]. \quad (7)$$

For a very rough surface with ks very large, $p \approx 1$, $g \approx 2.2$, and $x \approx 3$, in which case (5) reduces to

$$\sigma^s_{vv} = 2.2\,\cos^3\theta\,[\Gamma_v(\theta) + \Gamma_h(\theta)]\,, \text{for}\;\; ks >> 1. \quad (8)$$

The inclusion of the sum $[\Gamma_v(\theta) + \Gamma_h(\theta)]$ in the expression for σ^s_{vv} simply insures that for a very rough surface, $\sigma^s_{vv} = \sigma^s_{hh}$, and yet the magnitudes of these two copolarized coefficients are somehow related to the angle-dependent reflectivity of the surface.

To compare the proposed model with the experimental data (Fig. 8), we first normalized the measured values of σ^s_{vv} by dividing each by the sum of the reflectivities corresponding to the dielectric values associated with the surface and incidence angle and then plotted the results as a function of ks. The same normalization procedure was applied to (5) prior to plotting it in Fig. 8. In fact, the values of the coefficients appearing in (6) and (7) were selected by matching the expression given by (5) to the data.

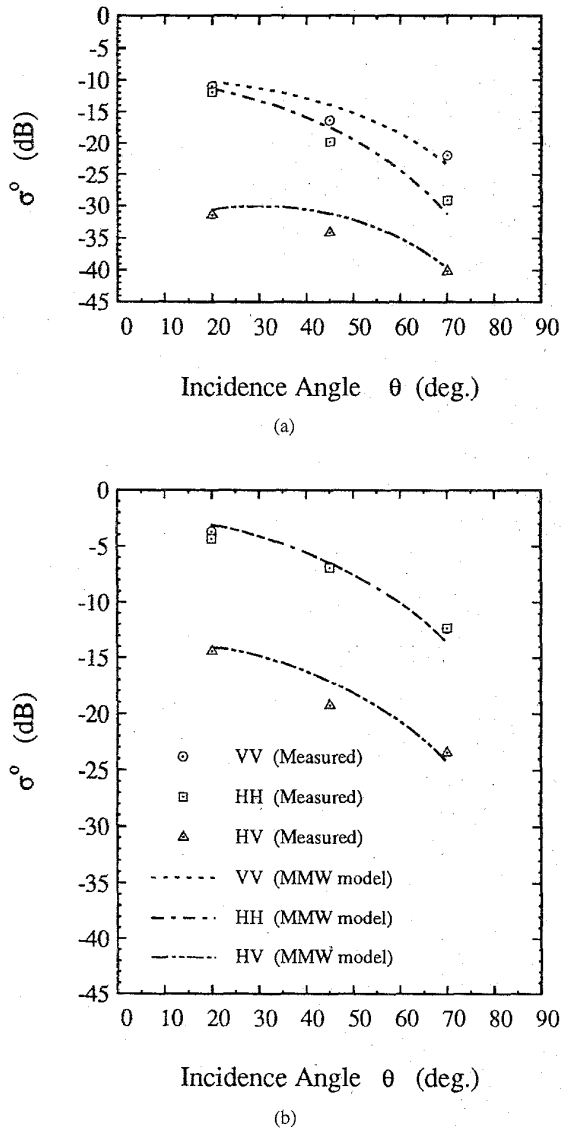

Fig. 6. Comparison of the measured backscattering coefficients for wet soil surfaces with calculations based on the semiempirical surface scattering model given in Section III for (a) the smoothest surface at 35 GHz ($ks = 0.48$), and (b) the roughest surface at 94 GHz ($ks = 15.3$).

D. Comparison of Model with Observations

The expressions given by (2)–(7) represent a semiempirical model for characterizing the surface-scattering component of millimeter-wave backscattering from a random rough surface. The continuous curves shown in Fig. 6 are based on this model as are the curves shown in Fig. 9 for surface S2 (with intermediate roughness) and in Fig. 10 where the model is compared with an independent data set (not used in constructing the surface model) reported by Yamasaki *et al.* [3] at 60 GHz, also for wet-soil surfaces.

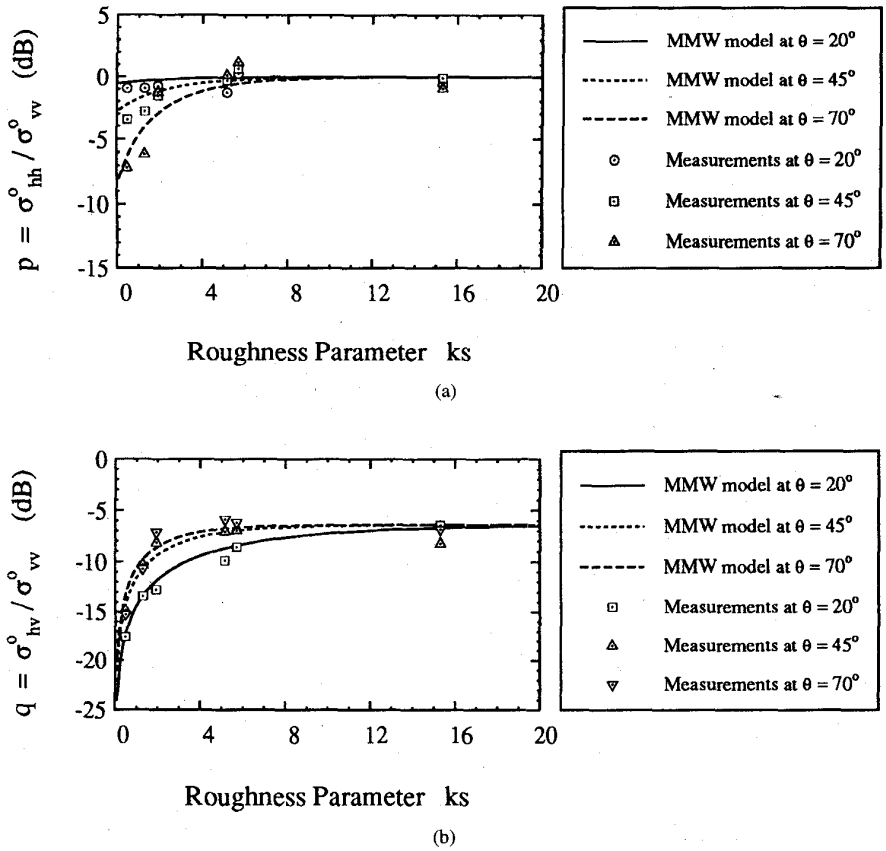

Fig. 7. Measured sensitivity of (a) the copolarized ratio p, and (b) the cross-polarized ratio q (normalized to $\sqrt{\Gamma_o}$) to surface roughness for wet soil surfaces at various incidence angles. The continuous curves are based on the expressions given in Section III.

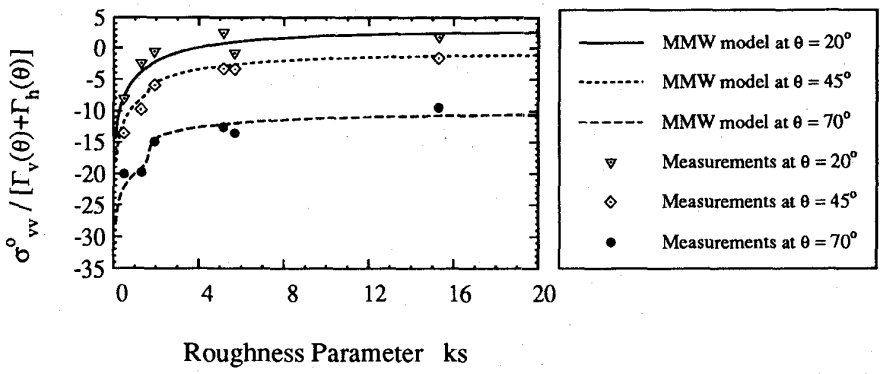

Fig. 8. The sensitivity of σ^o_{vv} to surface roughness for wet soils at various incidence angles.

IV. Volume Scattering

Before we embark on a detailed examination of σ^v, the volume backscattering contribution to the total backscattering coefficient σ^o, it would be instructive to examine the evidence we have in support of conducting such an examination in the first place. After all, studies conducted at centimeter wavelengths have shown that the behavior of the backscatter from random surfaces can be explained by surface scattering alone, without the need to add a volume-scattering contribution. The need to consider volume scattering at millimeter wavelengths can be illustrated through an examination of the experimental data shown in Fig. 11 which include a set of plots of σ^o_{hh} and σ^o_{hv} for a dry soil surface and another set for the same surface immediately after wetting the surface with a fine mist using a sprinkler system, thereby preserving the roughness of the surface. According to surface scattering models, both theoretical and empirical, increasing the soil moisture content causes the level of σ^o to increase at all angles of incidence for all polarization configurations. This is certainly not the behavior observed in Fig. 11. For HH polarization, σ^o_{hh} of the

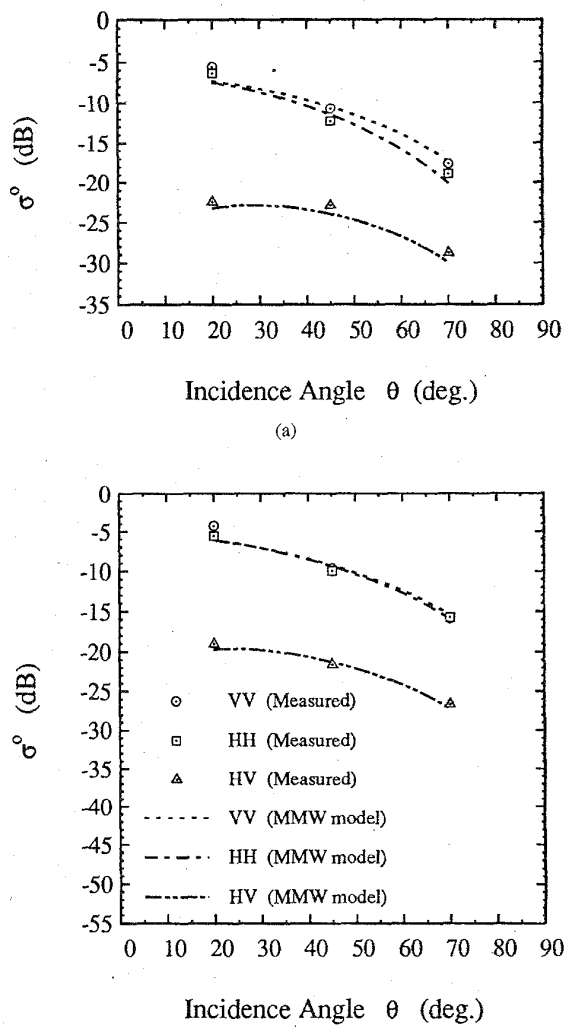

Fig. 9. Comparison between measured data of S2-wet soil surface and the MMW semiempirical surface scattering model at (a) 35 GHz and (b) 94 GHz.

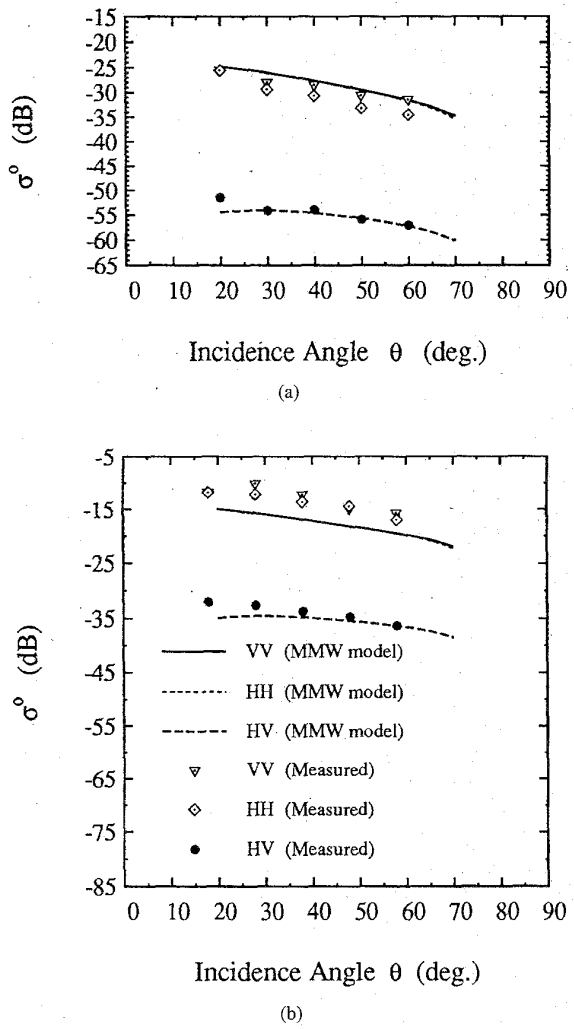

Fig. 10. Comparison between measured data for wet soil surfaces ($\epsilon_r = 1.9 + j\ 0.4$) at 60 GHz and the MMW semiempirical surface scattering model for (a) $ks = 0.16$ and (b) $ks = 1.75$. (Data from Yamasaki *et al.* [3]).

dry surface at $\theta = 20°$ is slightly lower than that for the wet surface, but at 70°, σ^o_{hh} for the dry soil surface is *higher* than that for the wet surface. A similar, but even more pronounced, behavior is observed for HV polarization. The explanation for these observations stems from the following properties.

1) Surface scattering increases with increasing moisture content (dielectric constant), as stated earlier.
2) For surface scattering, σ^s varies with θ as $\cos^3\theta$ to $\cos^4\theta$, depending on surface roughness.
3) Volume scattering decreases with increasing moisture content, in part because the air-soil transmission coefficient decreases with increasing moisture content and because the extinction in the soil medium increases rapidly with moisture content.
4) The volume scattering coefficients exhibit a very weak response as a function of the incidence angle θ.
5) The dimensions of the air voids (see Fig. 3(b)), which constitute the scattering particles in the soil medium, are such that the scattering is in the Rayleigh region, which exhibits a λ^{-4}–dependence. Consequently, volume scattering is insignificantly small at centimeter wavelengths, but becomes important at millimeter wavelengths when the soil surface is dry.

A. Radiative Transfer Theory

To compute the volume scattering contribution, we propose to use radiative transfer (RT) theory. As was noted earlier, the moisture content of the wet soils was essentially uniform with depth over the top four centimeters, but for the dry soils, the top surface layer, which was on the order of 1–3 cm thick, was very dry and the soil layer underneath it was generally fairly wet. Hence, we decided to model the soil medium as a thin layer of thickness h overlying a wet-soil half space. The thin layer, which is bounded by a random surface at the air-soil interface, contains air voids (scatterers) embedded in the soil background. From the measured surface profile,

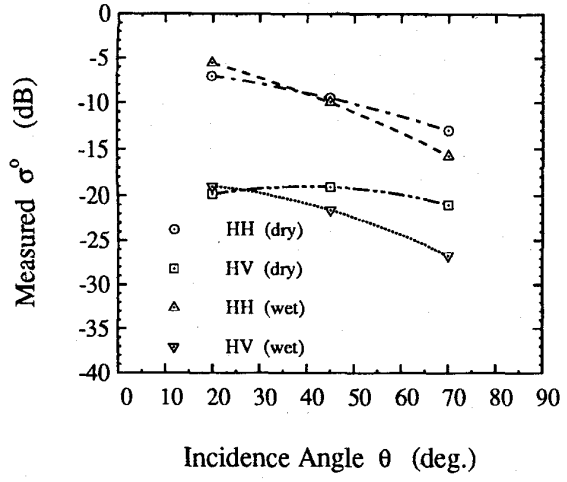

Fig. 11. Measured σ^o_{hh} and σ^o_{hv} for wet and dry surface conditions at 94 GHz ($ks = 5.16$). Note that at 70°, σ^o (dry) is greater than σ^o (wet) for both polarizations, evidence of volume scattering contribution.

extended into both the x- and y-dimensions, a probability density function is computed for the direction $\hat{n}$ of the local surface normal. For any specified direction of incidence $\hat{k_i}$, the dot product $(\hat{k_i}.\hat{n})$ determines the local angle of incidence θ_l. Hence, for any given radar incidence angle θ_i (measured relative to the normal to the mean surface), we generate a probability distribution for θ_l. Upon solving the radiative transfer equation numerically for Mie spherical particles using the technique outlined in Kuga *et al.* [10], the total volume scattering contributed by the layer is obtained by performing an incoherent addition of the volume scattering contributions emerging from all points on the surface, realized by weighing the contributions in accordance with the probability density function of θ_l. This approach is similar to that reported in [8] for computing surface scattering from tilted perturbed planes.

Solution of the radiative transfer equations requires knowledge of the void's shapes, sizes, volume fraction, and relative dielectric constant, in addition to the relative dielectric constants of both the background solid soil material and the wet soil half space. In this paper, we have assumed that the air voids are spherical in shape with a relative dielectric constant $\epsilon_a = 1.0 + j0.0$. The void-size distribution function shown in Fig. 3(b) was used in the solution of the RT equations for surfaces S1 and S2, and that corresponding to S3 (not shown) was used for the third surface. The relative dielectric constant of the background solid soil material was taken as $\epsilon_{ss} = 4.7$, based on the empirical formula $\epsilon_{ss} = (1.01+0.44\rho_{ss})^2 - 0.062$ reported in [9], where $\rho_{ss} = 2.65$ g/cm^3 is the measured solid soil density (which agrees well with ρ_{ss} of sandy soils [8], [9]). The effective dielectric for the wet soil half space was assumed to be $\epsilon_2 = 7.0 + j4.0$ at 35 GHz and $\epsilon_2 = 5.0 + j2.5$ at 94 GHz. The voids volume fractions given in Table II were calculated on the basis of the measured bulk densities and solid soil density, $\nu_a = 1 - \rho_b/\rho_{ss}$.

The results of this approach for computing the volume backscattering contribution σ^v are summarized in the next section. By way of examining the relative importance of

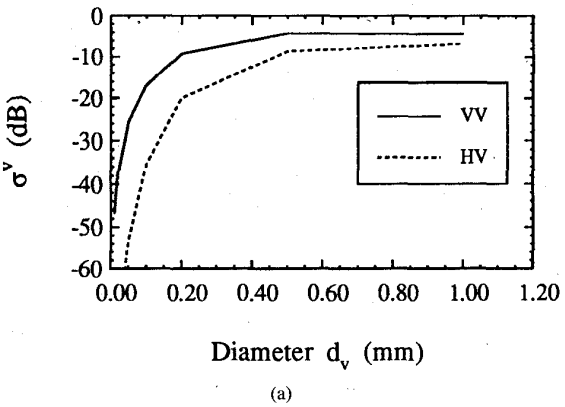

(a)

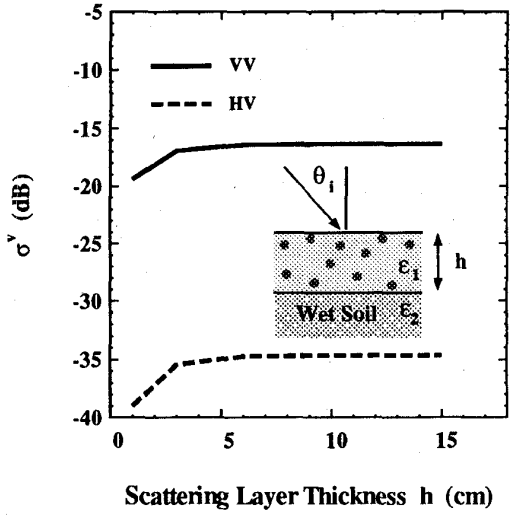

(b)

Fig. 12. Computed sensitivity of σ^v to (a) particle diameter (for layer thinkness $h = 3$ cm), and (b) scattering layer thickness (for particle diameter $d_v = 0.1$ mm). The computations were conducted at 94 GHz for an incidence angle $\theta = 20°$ and void volume fraction $\nu_a = 0.36$.

volume scattering, however, we calculated σ^v at 94 GHz for an upper layer containing air voids of uniform diameter, d_v. The results are shown in Fig. 12, which shows σ^v as a function of d_v for a thickness $h = 3$ cm, and as a function of h for a void diameter $d_v = 0.1$ mm. The responses to h (Fig. 12(b)) indicate that the thin surface layer "appears" semiinfinite in depth once its actual depth h exceeds about 3 cm. The variations of σ^v with d_v displayed in Fig. 12(a), which include both the Rayleigh and Mie regions, reaches saturation levels of about -4 dB for σ^v_{vv} and -7 dB for σ^v_{hv}. The saturation level for σ^v_{vv} is certainly comparable with or greater than the values measured for the wet soil surfaces at the same incidence angle and frequency, and for σ^v_{hv}, the saturation level is higher than all the wet-soil values of σ^v_{hv} displayed in Figs. 6, 9, and 10. Thus, the volume scattering contribution may indeed be a significant, or even the dominant, contribution depending on the void-size distribution. The volume scattering coefficients plotted in Fig. 12(a) approach the saturation stage when d_v exceeds 0.5 mm, which corresponds to $kr_v = kd_v/2 = \pi d_v\sqrt{\epsilon_r}/\lambda_o \simeq 0.86$, where λ_o is the free space wavelength (λ_o

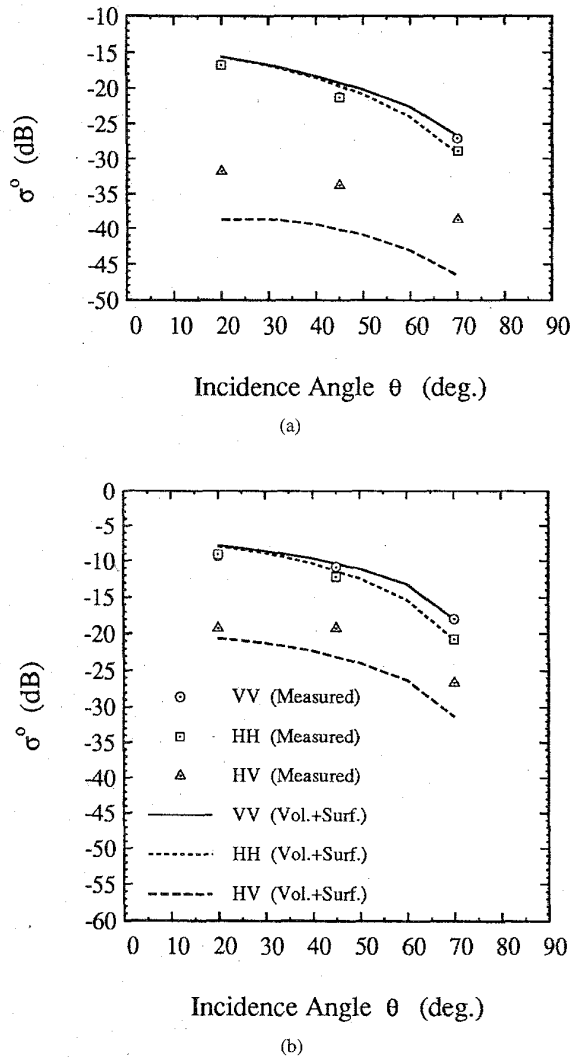

Fig. 13. Comparison between the measured backscattering coefficient and the total backscattering coefficient σ^o predicted by the sum of surface and volume scattering contributions for surface S1 at (a) 35 GHz and (b) 94 GHz.

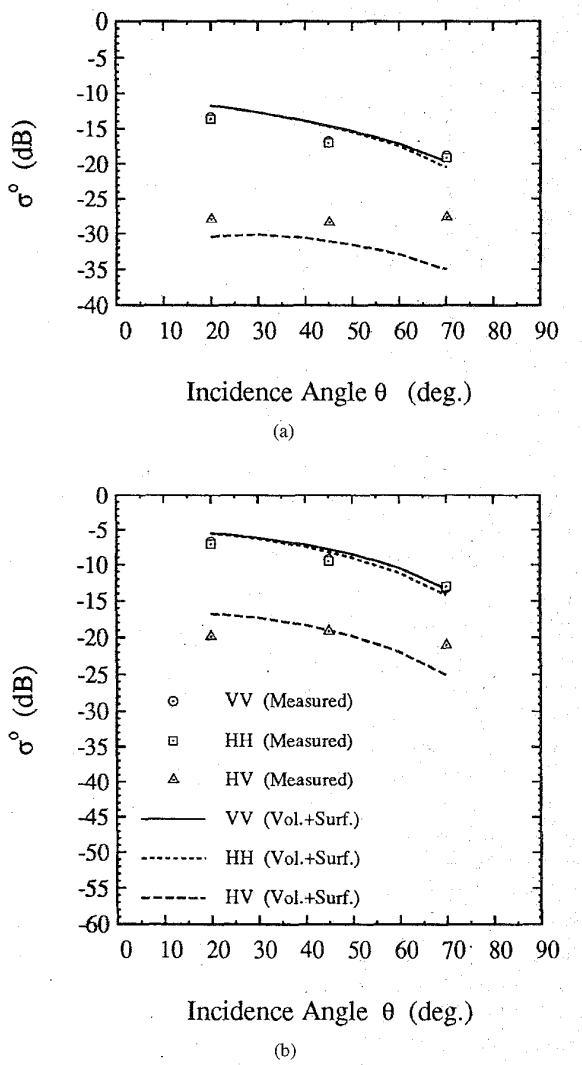

Fig. 14. Comparison between the measured backscattering coefficient and the total backscattering coefficient σ^o predicted by the sum of surface and volume scattering contributions for surface S2 at (a) 35 GHz and (b) 94 GHz.

= 3.2 mm at 94 GHz) and $\epsilon_r = 3.1$ is the effective dielectric constant of the dry soil background. The soils investigated in this study had void size distributions extending between 0.02 mm and about 0.4 mm, with the bulk of the voids having diameters smaller than 0.2 mm (see Fig. 3(b)).

B. Results

For the dry soil surfaces, the total backscattering coefficients σ^o_{ij} (i, $j = v$ or h) were computed according to (1) by adding incoherently the volume scattering contribution σ^v_{ij}, computed using the RT technique, to the surface scattering contribution σ^s_{ij}, calculated according to the empirical model described in the preceding section (see (2)–(7)). Good overall agreement is observed between the computed values of σ^o_{ij} and the measured radar responses for all surfaces at both frequencies, as can be seen in Figs. 13 through 15. In all cases, the thickness of the top dry soil surface layer was taken as 3 cm.

It must be pointed out that at 35 GHz, σ^o_{ij} is dominated by surface scattering with minimal contribution provided by volume scattering (σ^s_{ij} is typically larger than σ^v_{ij} by 10 dB). However, at 94 GHz, the volume scattering component is comparable to the surface scattering component for the copolarized scattering coefficients, as can be seen in Fig. 16(a), and for cross-polarization, σ^o_{hv} is dominated by the volume contribution (Fig. 16(b)).

C. Soil Moisture Dependence

The cases considered in this paper fall into two groups: a) wet soils, which may be defined as those with moisture contents exceeding 0.12 g/cm^3 in the top 1-cm layer, and b) dry soils, for which $m_v < 0.04$ g/cm^3 in the top 1-cm layer (see Table II). For the wet-soil group, our analysis shows that the volume-scattering contribution may be ignored and that the total backscatter is dominated by the surface-scattering

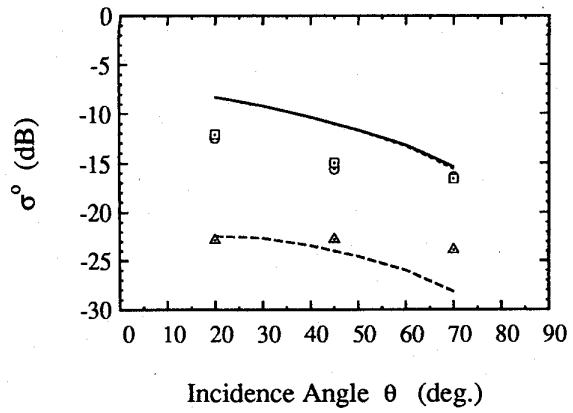

(a)

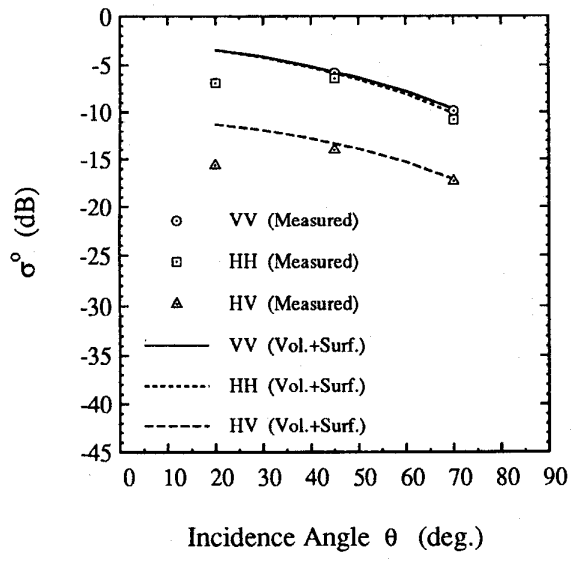

(b)

Fig. 15. Comparison between the measured backscattering coefficient and the total backscattering coefficient σ^o predicted by the sum of surface and volume scattering contributions for surface S3 at (a) 35 GHz and (b) 94 GHz.

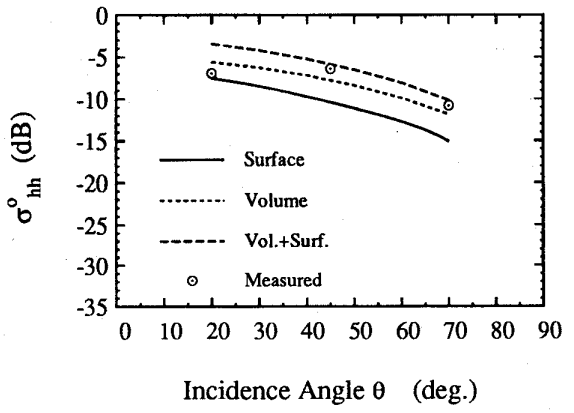

(a)

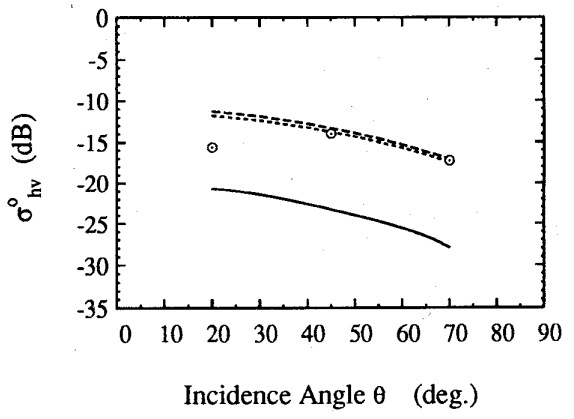

(b)

Fig. 16. Contributions of the surface-scattering component alone, the volume-scattering component alone, and the sum of both components for surface S3 at 94 GHz: (a) σ^o_{hh} (b) σ^o_{hv}.

component. The volume-scattering contribution is very small because at millimeter wavelengths the penetration depth is on the order of a few millimeters when $m_v > 0.1$ g/cm^3.

For the dry-soils group, the volume-scattering contribution was computed by assuming the top surface layer to be 3 cm in thickness and totally dry. Although the measured values of m_v were very small, they were not exactly zero over the top 3-cm layer (Table II). Nevertheless, they were assumed to be zero to simplify the calculation. A possible approach for modeling the dependence on moisture content is to treat the soil as a perfectly dry top surface layer of thickness h, overlying a very wet half-space, just as we have done in calculating the volume-scattering contributions for the dry soils examined in this study, but to also relate h to the average dielectric constant or moisture content of the upper 3-cm layer. Thus, h would vary from 3-cm for $m_v = 0$ down to zero thickness for $m_v = 0.15$ g/cm^3. These figures apply to 94 GHz and are at best a rough estimate based on radiative-transfer model calculations. Had we applied this approach to the calculations performed in connection with the dry soils, h would have been reduced from 3-cm down to about 2-cm, resulting in a change of about 1–2 dB in σ^v. Thus, verification of the applicability of such a model will have to await until further experimental investigations are performed for soils with moisture contents in the 0.04 to 0.15 g/cm^3 range.

V. Conclusion

The backscattering coefficients of three soil surfaces were measured as a function of incidence angle using two scatterometers operating at 35 GHz and 94 GHz. The soil surfaces, with roughnesses ranging between $ks = 0.48$ and $ks = 15.3$, were measured under wet and dry conditions. When compared to measurements, the physical optics and geometric optics surface-scattering models, as well as the empirical surface-scattering model given in [1], failed to consistently predict the measured backscattering coefficients.

Analysis of the measured radar data indicates that in general both surface and volume scattering contributions are present at MMW frequencies. For wet soil conditions, surface scattering is the dominant contribution and it can be modeled using a

set of semiempirical expressions. The volume contribution is important when the soil surface is dry, particularly at 94 GHz. Using radiative transfer theory, the volume scattering contribution was calculated by treating the soil medium as comprised of air voids imbedded in a soil background. This approach, which led to good agreement with the experimental observations, indicates that at 94 GHz, for example, the surface and volume scattering components are of comparable magnitude for σ^o_{vv} and σ^o_{hh}, but for the cross-polarized σ^o_{hv}, volume scattering is the dominant contribution.

REFERENCES

[1] Y. Oh, K. Sarabandi, and F. T. Ulaby, "An empirical and an inversion technique for radar scattering from bare soil surfaces," *IEEE Trans. Geosci. Remote Sensing*, vol. 30, pp. 370–381, Mar. 1992.

[2] ——, "An empirical model for phase difference statistics of rough surfaces," in *Proc. IGARSS '93 Symp.*, Tokyo, Japan, vol. III, pp. 1003–1005, Aug. 1993.

[3] H. Yamasaki, J. Awaka, A. Takahashi, K. Okamoto, and T. Ihara, "Measurements of soil backscatter with a 60 GHz scatterometer," *IEEE Trans. Geosci. Remote Sensing*, vol. 31, pp. 761–766, July 1992.

[4] F. T. Ulaby, M. Whitt, and K. Sarabandi, "AVNA-based polarimetric scatterometers," *IEEE Antennas Propagat. Mag.*, vol. 32, pp. 5–17, Oct. 1990.

[5] F. T. Ulaby and C. Elachi, *Radar Polarimetry for Geoscience Applications*. Norwood, MA: Artech House, 1990.

[6] J. B. Mead, "Polarimetric measurements of foliage and terrain at 225 GHz," Ph.D. dissertation, Univ. Massachusetts, Amherst, MA, 1990.

[7] K. Sarabandi, "Derivation of phase statistics of distributed targets from the averaged mueller matrix," *Radio Sci.*, vol. 27, pp. 553–560, Sept.-Oct. 1992.

[8] F. T. Ulaby, R. K. Moore, and A. K. Fung, *Microwave Remote Sensing*, vol. II-III. Norwood, MA: Artech House, 1986.

[9] M. C. Dobson, F. T. Ulaby, M. T. Hallikainen, and M. A. El-rayes, "Microwave dielectric behavior of wet soil-Part II: Dielectric mixing models," *IEEE Trans. Geosci. Remote Sensing*, vol. GRS-23, pp. 35–46, Jan. 1985.

[10] Y. Kuga, F. T. Ulaby, T. F. Haddock, and R. D. DeRoo, "Millimeter-wave radar scattering from snow 1. Radiative transfer model," *Radio Sci.*, vol. 26, pp. 329–341, Mar.-Apr. 1991.

Adib Nashashibi (S'82–M'95), photograph and biography not available at the time of publication.

Fawwaz T. Ulaby (M'68–SM'74–F'80), for a photograph and biography, see p. 99 of the January 1996 issue of this TRANSACTIONS.

Kamal Sarabandi (S'87–M'90–SM'93), for a photograph and biography, see this issue, p. 432.